# Glycogen Synthase Kinase-3α Limits Ischemic Injury, Cardiac Rupture, Post–Myocardial Infarction Remodeling and Death

Hind Lal, PhD; Jibin Zhou, MD, PhD; Firdos Ahmad, PhD; Raihana Zaka, PhD; Ronald J. Vagnozzi, BS; Morgan DeCaul, BS; James Woodgett, PhD; Erhe Gao, MD, PhD; Thomas Force, MD

***Background***—The molecular pathways that regulate the extent of ischemic injury and post–myocardial infarction (MI) remodeling are not well understood. We recently demonstrated that glycogen synthase kinase-3α (GSK-3α) is critical to the heart's response to pressure overload. However, the role, if any, of GSK-3α in regulating ischemic injury and its consequences is not known.

***Methods and Results***—MI was induced in wild-type (WT) versus GSK-3α$^{(-/-)}$ (KO) littermates by left anterior descending coronary artery ligation. Pre-MI, WT, and KO hearts had comparable chamber dimensions and ventricular function, but as early as 1 week post-MI, KO mice had significantly more left ventricular dilatation and dysfunction than WT mice. KO mice also had increased mortality during the first 10 days post-MI (43% versus 22%; $P=0.04$), and postmortem examination confirmed cardiac rupture as the cause of most of the deaths. In the mice that survived the first 10 days, left ventricular dilatation and dysfunction remained worse in the KO mice throughout the study (8 weeks). Hypertrophy, fibrosis, and heart failure were all increased in the KO mice. Given the early deaths due to rupture and the significant reduction in left ventricular function evident as early as 1 week post-MI, we examined infarct size following a 48-hour coronary artery ligation and found it to be increased in the KO mice. This was accompanied by increased apoptosis in the border zone of the MI. This increased susceptibility to ischemic injury–induced apoptosis was also seen in cardiomyocytes isolated from the KO mice that were exposed to hypoxia. Finally, Bax translocation to the mitochondria and cytochrome C release into the cytosol were increased in the KO mice.

***Conclusion***—GSK-3α confers resistance to ischemic injury, at least in part, via limiting apoptosis. Loss of GSK-3α promotes ischemic injury, increases risk of cardiac rupture, accentuates post-MI remodeling and left ventricular dysfunction, and increases the progression to heart failure. These findings are in striking contrast to multiple previous reports in which deletion or inhibition of GSK-3β is protective. **(*Circulation*. 2012;125:65-75.)**

**Key Words:** GSK-3α ■ myocardial infarction ■ heart failure ■ cardiac remodeling

Post–myocardial infarction (MI) remodeling is the leading cause of advanced left ventricular (LV) dysfunction and heart failure in the developed world.[1,2] However, the molecular pathways regulating ischemic injury and remodeling are not well understood.[3] We recently reported that mice with deletion of glycogen synthase kinase (GSK)-3β specifically in cardiomyocytes had less post-MI remodeling and apoptosis in the remote myocardium, and had better-preserved LV function in comparison with wild-type mice.[4] However, the role played by the other GSK-3 isoform, GSK-3α, in the ischemic heart has not, to our knowledge, been studied. Progress in this area has been slow, in part, because, with the exception of gene deletion, none of the strategies previously used to inhibit GSK-3 activity in vivo are isoform specific and the majority (eg, small-molecule inhibitors or overexpression of dominant inhibitory mutants) typically impact other protein kinases in addition to GSK-3s.[5,6] Webb et al[7] used a gain-of-function approach to address the role of GSK-3s in post-MI remodeling and, in contrast with our results in the GSK-3β KO, concluded that remodeling post-MI was not regulated by GSK-3s. However, this knock-in mouse contained mutations that led to constitutive activity of both GSK-3 isoforms. Thus, if the 2 GSK-3 isoforms have opposing effects on remodeling, this might not be detected in the double knock-in model.

Received June 18, 2011; accepted November 2, 2011.

From the Center for Translational Medicine & Cardiology Division, Thomas Jefferson University, Philadelphia, PA (H.L., J.Z., F.A., R.Z., R.J.V., M.D., E.G., T.F.); and Samuel Lunenfeld Research Inst, Mount Sinai Hospital, Toronto, ON, Canada (J.W.).

**The online-only Data Supplement is available with this article at http://circ.ahajournals.org/lookup/suppl/doi:10.1161/CIRCULATIONAHA.111.050666/-/DC1.**

Correspondence to Thomas Force, MD, Center for Translational Medicine, Thomas Jefferson University, College Building, Rm 316, 1025 Walnut St., Philadelphia, PA 19107. E-mail thomas.force@jefferson.edu



*Circulation* **is available at http://circ.ahajournals.org** **DOI: 10.1161/CIRCULATIONAHA.111.050666**

## Clinical Perspective p 75

We felt that understanding the role played by GSK-3$\alpha$ was important, because significant concerns have recently been raised over adverse effects in the heart following deletion of GSK-3$\alpha$.[8] Specifically, we found that, although the deletion of GSK-3$\beta$ had little effect on remodeling following pressure overload, deletion of GSK-3$\alpha$ led to increased hypertrophy and more pronounced LV dysfunction following thoracic aortic constriction. Given that inhibitors of GSK-3 are in development for a host of disease states, including diabetes and other diseases that are associated with significant cardiovascular comorbidities because of the relatively advanced age of the patients (eg, Alzheimer disease and Parkinson disease),[9–12] we felt it was important from a clinical perspective to clarify the role of GSK-3$\alpha$ in the ischemic heart. Herein, we report that deletion of GSK-3$\alpha$ leads to increased risk of cardiac rupture and death. The KO mice that survive have worse remodeling and LV dysfunction. Surprisingly, given that the model used was permanent coronary artery occlusion, infarct size was increased in the KO, at least in part, because of increased apoptosis. This finding was associated with alterations in prosurvival signaling pathways, increased Bax translocation, and cytochrome C release. In summary, we have identified several novel processes regulated by GSK-3$\alpha$ including resistance to ischemic injury and post-MI remodeling. These cardioprotective effects of GSK-3$\alpha$ in the setting of ischemia and infarction appear to be substantial.

## Materials and Methods

### Antibodies and Chemicals

Antibodies used were directed against AKT phosphorylated at Ser473 (No. 4051), AKT phosphorylated at Thr308 (No. 9275), AKT (No. 9272), AMPK phosphorylated at Thr172 (No. 2531), AMPK (No. 2603), p38 MAPK phosphorylated at Thr180/Tyr182 (No. 9211), Bax (No. 2772), voltage-depended anion channel (No. 4661) (all from Cell Signaling, Danvers, MA). $\alpha$-Smooth muscle actin ($\alpha$-SMA) antibody (No. A5228) was from Sigma-Aldrich, St. Louis, MO. p38 MAPK antibody (No. sc-535) and cytochrome C (No. sc-13156) were from Santa Cruz Biotechnology, Santa Cruz, CA. The protease and phosphatase inhibitor cocktails (Nos. P8430, P2850) were from Sigma, St. Louis, MO.

### Myocardial Infarction

Following baseline echocardiography, permanent occlusion of the proximal left anterior descending coronary artery was performed in wild-type (WT) versus GSK-3$\alpha^{(-/-)}$ (KO) male littermates, exactly as described.[13] Echocardiography was repeated at 1, 2, 4, and 8 weeks post-MI. After the 8-week echo examination, mice were euthanized for the studies outlined below.

### Echocardiography

Transthoracic two-dimensional echocardiography was performed with a 12-mHz probe (Visualsonics) on mice anesthetized by inhalation of isoflurane (1–1.5%). M-mode interrogation was performed in the parasternal short-axis view at the level of the greatest LV end-diastolic dimension. LV end-diastolic dimension, LV end-systolic dimension, and septal and LV posterior wall thicknesses were determined and used to calculate the percentage of fractional shortening, ejection fraction, and LV mass.[14] Fractional shortening was calculated with the formula: $[(LVEDD-LVESD)/LVEDD]\times100$, where LVEDD is LV end-diastolic dimension, and LVESD is LV end-systolic dimension. The ejection fraction was calculated with the formula: $[(LVEDV-LVESV)/LVEDV]\times100$, where EDV is end-diastolic volume and ESV is end-systolic volume.[15,16] LV mass was calculated with the formula: $[(2\times PWT)+EDD]^3-EDD^3$, where EDD is end-diastolic dimension and PWT is posterior wall thickness.

### Determination of LV Infarct Size

Myocardial infarct size was determined as previously described.[13,17] In brief, at 48 hours post-MI, mice were euthanized and the heart was quickly excised and sliced into five 1.0-mm-thick sections perpendicular to the long axis of the heart. The sections were then incubated with 1% triphenyltetrazolium chloride (Sigma) in phosphate-buffered saline (pH 7.4) for 15 minutes at room temperature and then were photographed. For infarct size at 48 hours post-MI, triphenyltetrazolium chloride-stained area, and triphenyltetrazolium chloride-negative area (infarcted myocardium) were measured by the use of ImageJ software. Myocardial infarct size was expressed as a percentage of total LV area.

### Histological Analysis

LV tissue was fixed with 4% paraformaldehyde for 24 hours, dehydrated through increasing concentrations of ethanol, and then embedded in paraffin.[18] LV sections (5 $\mu$m) were stained with hematoxylin-eosin (Sigma-Aldrich) or Masson trichrome (Sigma-Aldrich). A Nikon Eclipse 80i microscope and NIS Elements software were used to record images. Cross-sectional area of hematoxylin-eosin-stained cardiomyocytes was determined with the use of NIS Elements software. In addition, NIS Elements software was used to analyze the total area of fibrosis on trichrome-stained sections. All analyses were performed by an observer blinded to the conditions.

### Determination of Myocardial Apoptosis

*In Situ* Cell Death Detection kit, TMR red (Roche No. 12 156 792 910) was used for terminal deoxynucleotidyl-transferase–mediated dUTP nick-end labeling (TUNEL). The LV sections were treated according to the manufacturer's instructions, and slides were covered with a glass cover slide applied with mounting media containing 4,6-diamidino-2-phenylindole. A Nikon Eclipse 80i microscope was used to visualize the cells, and NIS Elements software was used to record images. The percentage of TUNEL-positive nuclei (of $>$3000 total nuclei per heart) was determined in the myocardium remote from the infarct zone of each animal.

### Adult Mouse Cardiac Myocyte Isolation and Culture

Adult mouse cardiac myocytes were isolated and cultured by using a modification of the collagenase dissociation method as described.[19] Mice were treated with heparin (50 U) and anesthetized by intraperitoneal injection of Avertin. The heart was quickly excised and the aorta cannulated for retrograde perfusion in a Langendorff apparatus at a constant flow rate of 3 mL/min at 37°C. The heart was perfused for 5 minutes with isolation buffer (120 mmol/L NaCl, 5.4 mmol/L KCl, 1.2 mmol/L $MgSO_4$, 1.2 mmol/L $NaH_2PO_4$, 5.6 mmol/L glucose, 5 mmol/L $NaHCO_3$, 10 mmol/L HEPES, 50 $\mu$mol/L $CaCl_2$, 10 mmol/L 2,3-butanedione monoxime and 5 mmol/L taurine followed by digestion for 13 minutes with collagenase II (1.5 mg/mL, Worthington, Lakewood, NJ) in isolation buffer. After digestion, the heart was removed, and myocytes were suspended in isolation buffer. A series of 4 centrifugations and resuspensions were used for stepwise $Ca^{2+}$-reintroduction from 50 $\mu$mol/L to 1.0 mmol/L.

The cells were suspended in MEM with Hanks' buffered salt solution (HBSS), 100 U/mL penicillin, 2 mmol/L glutamine, 2 mmol/L Na-ATP, 10 mmol/L butanedione monoxime, and 10% calf serum. Isolated cardiac myocytes were plated for 2 hours on chamber slides coated with 10 $\mu$g/mL laminin. After this period of attachment, the medium was changed to MEM/HBSS containing 100 U/mL penicillin, 1$\times$ ITS (Sigma No. 13146), 10 mmol/L butanedione monoxime, glutamate, 2 mmol/L 0.1% BSA, and 10% calf serum, and incubated overnight at 37°C in a humidified atmosphere of 1% $CO_2$ and air.

### Hypoxia Protocol, Adenylate Kinase (AK) Release and TUNEL Assay

Experiments were performed the day after isolation and culture. Medium was serum-free, glucose-free MEM with HBSS that did not contain butanedione monoxime. This medium was preequilibrated overnight in the anaerobic chamber containing 1% $CO_2$ and 99% $N_2$. Cells were cultured for 4 hours in an In vivo$_2$ Hypoxia Workstation (Ruskinn) with a mixture of 1% $O_2$, 5% $CO_2$, and 93% $N_2$. Cells were then processed for TUNEL staining with the use of the *In Situ* Cell Death Detection kit, TMR red as described by the manufacturer (Roche No. 12 156 792 910). Slides were covered with a glass cover slide applied with mounting media containing 4,6-diamidino-2-phenylindole. A Nikon Eclipse 80i microscope was used to visualize the cells, and NIS Elements software was used to record images. TUNEL-positive nuclei were then expressed as a percentage of total nuclei. Release of adenylate kinase into the culture medium was measured in culture supernatants by a bioluminescent Toxilight kit (Lonza No. LT07-217) according to the manufacturer's instructions.

### Isolation of Mouse Heart Mitochondria

Mouse heart mitochondria were isolated as previously described.[20,21] WT and GSK-3α mice (8–10 weeks old) were anesthetized by intraperitoneal injection with Avertin, and the heart was quickly excised. The heart was minced on ice, resuspended in 1 mL of homogenization buffer (10 mmol/L tris, 250 mmol/L sucrose, 1× protease inhibitor, pH 7.5) supplemented with 1 mmol/L EDTA, and homogenized with a glass Dounce homogenizer and Teflon pestle. Homogenates were centrifuged at 1000 *g* for 5 minutes at 4°C. The supernatant was recentrifuged at 10 000 *g* for 15 minutes to pellet the mitochondria. Pellet was washed twice with homogenization buffer (without EDTA). The supernatant was recentrifuged at 50 000 rpm for 1 hour, and the resultant supernatant was used as cytosolic fraction.

### Isolation and Culture of Adult Cardiac Fibroblasts

Adult cardiac fibroblasts were isolated from 2- to 3-month-old WT and GSK-3α mice as described.[22] Hearts were excised, rinsed in cold Hank's balanced salt solution, minced, and digested with type II collagenase (1.5 mg/mL) (Worthington) and pancreatin (0.6 mg/mL) (Sigma) at 37°C for 15 minutes. The first digestion was discarded. The collagenase medium from the second digestion containing the cardiac fibroblasts was centrifuged for 10 minutes at 180 *g* and resuspended in DMEM with 10% fetal bovine serum/1% antibiotic solution. The digestion was repeated until the digestion fluid became clear (5–6 times). Cells were plated in 60-mm dishes (Corning, NY) and allowed to attach for 45 minutes before the first media change, which removed weakly adherent cells, including myocytes and endothelial cells. Fibroblasts were washed twice with $Ca^{2+}$- and $Mg^{2+}$-free PBS (Cellgro, Mediatech, Inc), trypsinized (Invitrogen), and passaged as required on the basis of cellular confluence.

### RNA Isolation, Reverse Transcription, and Quantitative Real-Time Reverse Transcribed Polymerase Chain Reaction

Total heart RNA was isolated by the use of a commercially available kit (Totally RNA, Ambion). First-strand cDNA was reverse transcribed with random hexamer primer with the use of the High Capacity cDNA RT kit (ABI, Carlsbad, CA). Real-time polymerase chain reaction (PCR) for atrial natriuretic peptide and brain natriuretic peptide was carried out in a MX3005P (Stratagene) thermocycler with the use of Taqman Universal PCR Master Mix and TaqMan gene expression assays (ABI, Carlsbad, CA; Assay ID: Mm01255748_g1 and Mm00435304_g1, respectively). β-Myosin heavy chain, collagen-1 and 18S rRNA amplification was performed with the use of QuantiTect SYBR Green Master Mix (Qiagen, Valencia, CA), and, after each run, a melting curve was acquired by heating the product to 95°C, cooling to and maintaining at 55°C for 20 seconds, then slowly (0.5°C/s) heating to 95°C, to determine the specificity of the PCR products. 18S rRNA levels did not differ between groups and were used for normalization. Relative gene expression was determined by using the δ-δ Ct method.

### Statistics

Differences between data groups were evaluated for significance by the use of the unpaired *t* test or 1-way analysis of variance, as appropriate and Bonferroni post test (Graph Pad prism Software Inc., San Diego, CA). Repeated-measures analysis of variance was used to evaluate the statistical significance of data acquired from the same animal over multiple time points. Survival analysis was performed by the Kaplan-Meier method, and between-group differences in survival were tested by the Gehan-Breslow-Wilcoxon test. Data are expressed as mean±SEM, unless noted otherwise. For all tests, a probability value of $\leq 0.05$ was considered to denote statistical significance.

## Results

### Deletion of GSK-3α Increases Post-MI Mortality

The creation of the GSK-3α KO mouse was previously described.[8,23] GSK3α KO mice appear normal at birth.[18] Ventricular function and chamber dimensions are normal at 3 months of age in the KO (online-only Data Supplement Figure I). We chose to study mice at 2 months of age with the termination of the experiments at or before 4 months of age, because they begin to develop cardiac hypertrophy at 4 months. WT and KO male mice were subjected to permanent ligation of the left coronary artery. There was no compensatory upregulation of GSK-3β in the heart after deletion of *Gsk3a* either at baseline or post-MI (data not shown). KO mice had significantly increased mortality during the first 10 days post-MI (43% versus 22% for littermate controls; $P=0.04$) (Figure 1A). Postmortem examination confirmed cardiac rupture as the cause of most of the deaths. In the mice that survived the first 10 days, there were no differences in mortality between WT and KO up to the termination of the study. Given the early increase in rupture, we asked whether ischemic injury might be increased in the KO mice. To assess this, we examined infarct size at 48 hours post–coronary artery ligation. We found that infarct size was indeed significantly increased in KO in comparison with WT mice (Figure 1B).

### GSK-3α Deletion Worsens LV Remodeling and Functional Deterioration Following Myocardial Infarction

We then examined the consequences of the increased ischemic injury in the KO mice. To determine the role of GSK-3α in myocardial remodeling, WT and GSK-3α KO male mice were subjected to MI at 2 months of age. Postinfarct ventricular remodeling in WT and KO mice was assessed with serial echocardiography. Pre-MI, WT and KO hearts had comparable chamber dimensions and ventricular function, but as early as 1 week post-MI, KO animals had a significantly greater increase in end-diastolic and end-systolic dimensions in comparison with WT animals, reflecting accelerated dilatative remodeling in the KO (Figure 2A and 2B). This was associated with marked LV dysfunction as reflected by reduced LVEF and LVFS (Figure 2C and 2D). LV dilatation and dysfunction remained more marked in the KO up to the termination of the study (8 weeks) (Figure 2). The increased remodeling in the KO was not due to the adverse effects of GSK-3α deletion in endothelial cells, because

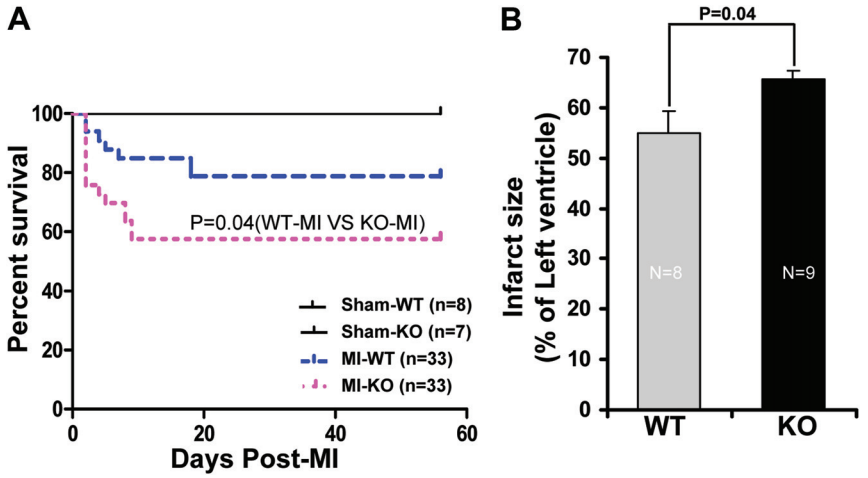


**Figure 1.** Deletion of GSK-3$\alpha$ increases ischemic injury and mortality post-MI. **A**, WT and GSK-3$\alpha$ KO mice were subjected to MI or sham surgery and survival was monitored for 8 weeks. Survival was analyzed by the Kaplan-Meier method, and differences between groups were determined by the Gehan-Breslow-Wilcoxon test. **B**, Two-month-old WT and KO mice were subjected to left coronary artery ligation or sham surgery. At 48 hours postligation, myocardial infarct size was determined by triphenyltetrazolium chloride staining. Infarct size was quantified and expressed as a percentage of the total area of the LV myocardium. Differences between groups were determined by unpaired *t* test, and results are expressed as means±SEM. A probability value of ≤0.05 was considered to denote statistical significance. MI indicates myocardial infarction; WT, wild type; KO, GSK-3$\alpha^{(-/-)}$; LV, left ventricular.

there was a modest but not statistically significant ($P=0.056$) increase in the capillary density in the KO (online-only Data Supplement Figure II). Myocardial inflammatory cell infiltration also appeared to play no role, because macrophage and neutrophil numbers were comparable in WT and KO mice at 24 hours post-MI (online-only Data Supplement Figures III and IV).

## GSK-3$\alpha$ KO Mice Display Increased Pathological Hypertrophy Post-MI

Three weeks after MI, mice were analyzed for morphometrics. Heart weight (HW), lung weight (LW), and body weight (BW) were determined, and HW/BW and LW/BW (the primary morphometric measures of hypertrophy and heart failure, respectively) were calculated. There were no



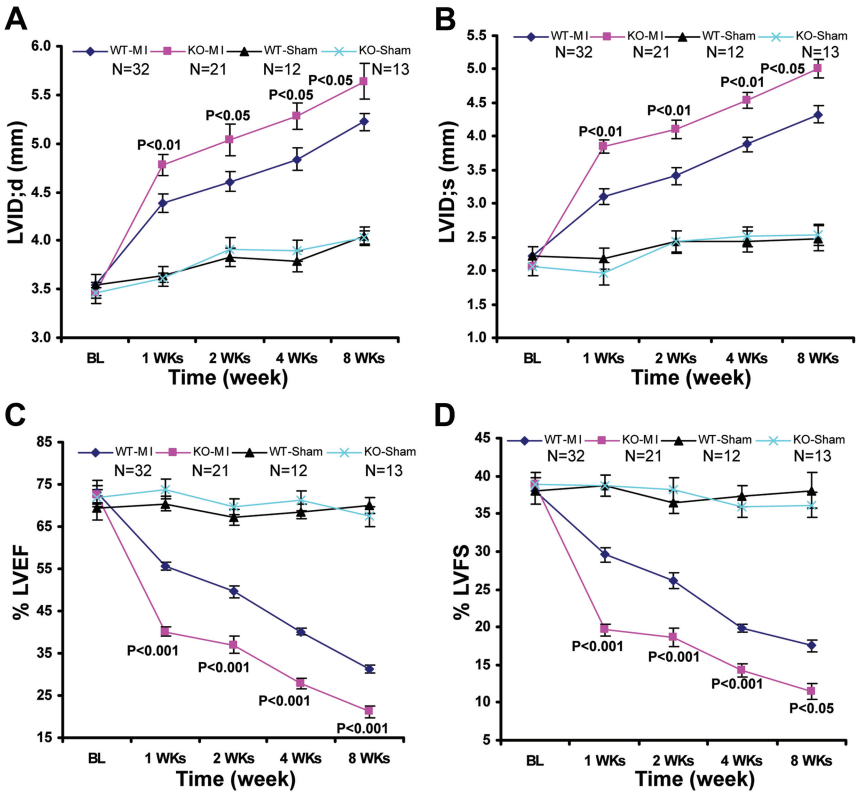


**Figure 2.** Deletion of GSK-3$\alpha$ increases dilatative remodeling and cardiac dysfunction post-MI. Two-month-old WT and GSK-3$\alpha$ KO mice underwent baseline transthoracic echocardiographic examination. Twenty-four hours later they were subjected to occlusion of the proximal left anterior descending coronary artery. Mice were then followed with echocardiography at the time points shown. **A**, Left ventricular internal dimension at end-diastole (LVID;d). **B**, LVID at end-systole (LVID;s). **C**, left ventricular ejection fraction (LVEF). **D**, LV fractional shortening (LVFS). Repeated-measures analysis of variance was used to evaluate the statistical significance, and results are expressed as means±SEM. A probability value of ≤0.05 was considered to denote statistical significance. Probability values are for the comparison of WT versus KO mice subjected to MI. MI indicates myocardial infarction; WT, wild type; KO, GSK-3$\alpha^{(-/-)}$.

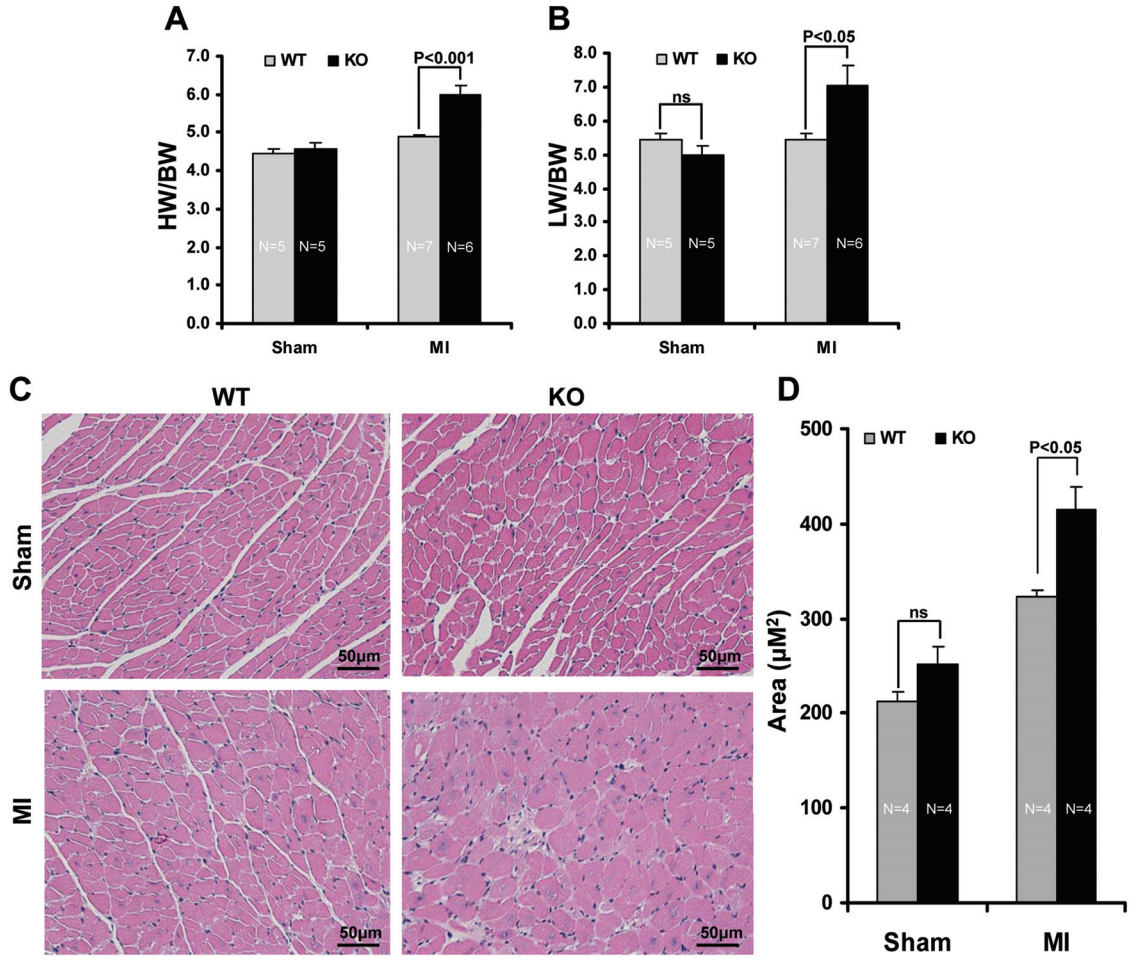


**Figure 3.** Deletion of GSK-3α leads to cardiac and cardiomyocyte hypertrophy post-MI. Two-month-old WT and GSK-3α KO mice were subjected to MI or sham surgery for 3 weeks, as described in Materials and Methods. **A**, Increased hypertrophy in the KO mice subjected to coronary artery ligation as shown by HW/BW ratio. **B**, Increased HF in the KO mice. The ratio of lung weight to body weight (LW/BW, a measure of heart failure) was significantly increased in the KO mice. **C**, Representative images of LV remote myocardium 8 weeks post-MI stained with hematoxylin-eosin. **D**, Quantification of cardiomyocyte CSA. For determination of CSA, a minimum of 100 cardiomyocytes per heart were measured. Differences between groups were determined by unpaired *t* test, and results are expressed as means±SEM. A probability value of ≤0.05 was considered to denote statistical significance. MI indicates myocardial infarction; WT, wild type; KO, GSK-3$\alpha^{(-/-)}$; CSA, cross-sectional area; HW, heart weight; LW, lung weight; BW, body weight.

significant differences at baseline between WT and KO. At 3 weeks post-MI, both HW/BW and LW/BW were significantly elevated in GSK-3α KO mice, suggesting increased post-MI hypertrophy and heart failure in GSK-3α–deficient hearts (Figure 3A and 3B). To examine hypertrophy at the cellular level, we measured cross-sectional area of hematoxylin/eosin-stained LV sections. Cross-sectional area was significantly increased in GSK-3α KO cardiomyocytes, confirming increased hypertrophic remodeling in the KO (Figure 3C and 3D). Next, we examined the reexpression of fetal genes as a marker of pathological hypertrophy and found a significant increase in atrial natriuretic peptide and β-myosin heavy chain at 3 weeks post-MI, further confirming increased pathological remodeling in the KO mice (Figure 4A and 4C). In addition, brain natriuretic peptide, a biomarker of heart failure, was also increased in the GSK-3α KO hearts (Figure 4B), consistent with the LW/BW data above.

## Deletion of GSK-3α Increased Post-MI Fibrosis, Extracellular Matrix Remodeling, Myofibroblast Activation, and Apoptosis in the Remote Myocardium

The extent of myocardial fibrosis was determined by using Masson trichrome staining of histological sections at 8 weeks post-MI. We observed a very marked increase in fibrosis in the remote (noninfarct) region in the KO hearts (Figure 5A and 5B). Next, we isolated RNA from the remote myocardium 3 weeks post-MI for quantification by real-time PCR of collagen-1 gene expression. Expression of collagen-1 was significantly upregulated in GSK-3α KO hearts (Figure 5C). The increase in collagen-1 gene expression is consistent with the increased fibrosis seen in the GSK-3α KO hearts. Because the myofibroblast is a primary contributor to extracellular matrix deposition and scar formation following MI, we next determined the role of GSK-3α in myofibroblast activation. Adult LV fibroblasts were isolated from WT and GSK-3α KO hearts as described in Materials and Methods.

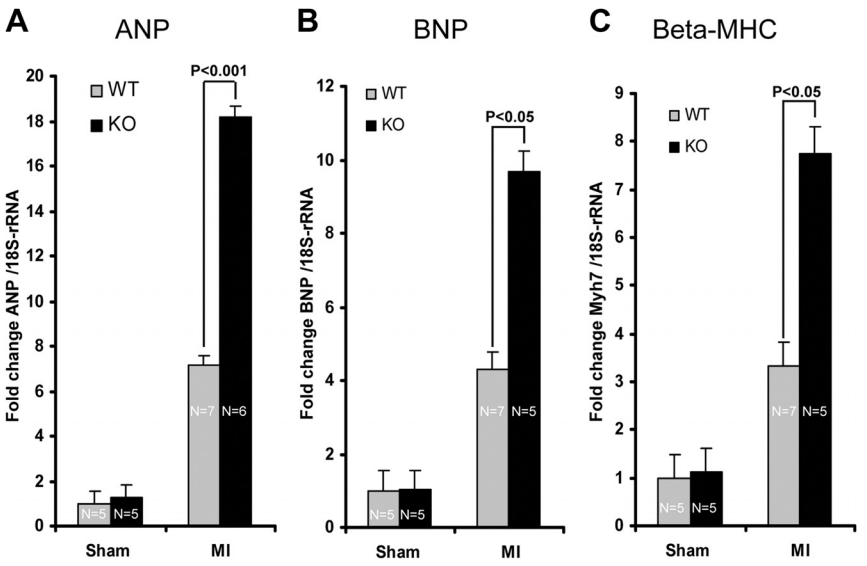


**Figure 4.** Reactivation of fetal gene expression in the GSK-3$\alpha$ KO mice post-MI. Transcripts of markers of pathological hypertrophy—**A**, atrial natriuretic peptide (ANP); **B**, brain natriuretic peptide (BNP); **C**, Myh7 ($\beta$-myosin heavy chain)—were increased in hearts from GSK-3$\alpha$ KO mice as determined by quantitative PCR, 21 days post-MI. Values indicate relative expression levels in comparison with the WT sham-operated group ($\pm$SEM). All values were normalized to 18S rRNA levels. Differences between groups were determined by unpaired *t* test, and results are expressed as means$\pm$SEM. A probability value of $\leq$0.05 was considered to denote statistical significance. MI indicates myocardial infarction; WT, wild type; KO, GSK-3$\alpha^{(-/-)}$; ANP, atrial natriuretic peptide; BNP, brain natriuretic peptide; PCR, polymerase chain reaction.

Previous studies have shown that fibroblasts spontaneously differentiate into myofibroblasts in culture, and this is associated with an increase in $\alpha$-SMA expression.[24] We confirmed that fibroblasts spontaneously underwent this differentiation under normal culture conditions as shown by enhanced $\alpha$-SMA expression with increasing passage. To determine the role of GSK-3$\alpha$ in myofibroblast differentiation, $\alpha$-SMA expression was examined at 72 hours. We found that $\alpha$-SMA expression increased in a time-dependent manner, and this increase was significantly enhanced in GSK-3$\alpha$ null

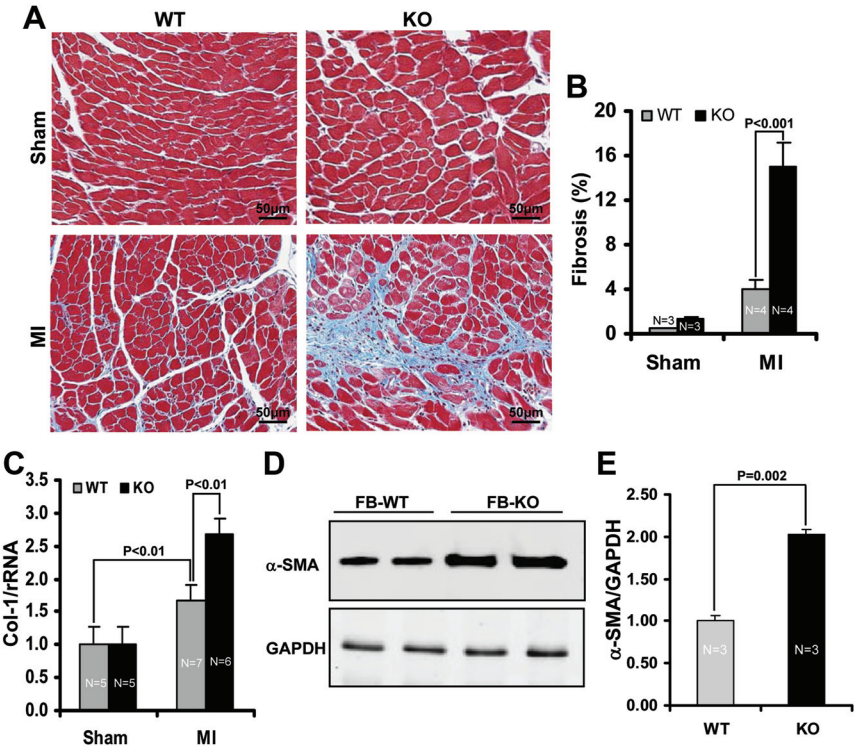


**Figure 5.** Deletion of GSK-3$\alpha$ exaggerates cardiac fibrosis, extracellular matrix remodeling, and myofibroblast activation. **A**, Fibrosis is increased in the KO mice post-MI. Representative images of LV remote myocardium in WT and KO stained with Masson trichrome 8 weeks post-MI. **B**, The percentage of LV myocardium with fibrosis was determined from 10 random images taken from each animal. **C**, Transcripts for collagen-1, a marker of extracellular matrix remodeling, in hearts from WT and GSK-3$\alpha$ KO mice were detected by quantitative PCR, 21 days post-MI. Values indicate relative expression versus WT sham-operated group ($\pm$SEM). All values were normalized to 18S rRNA levels. **D**, Adult fibroblasts were isolated from 3-month-old WT and GSK-3$\alpha$ KO mice. After 3 passages, cells were harvested and Western blotting was performed. Representative immunoblots showing increased $\alpha$-SMA expression in fibroblasts from GSK-3$\alpha$ KO mouse hearts indicates increased myofibroblast activation in KO mouse hearts. **E**, Quantification of $\alpha$-SMA expression in GSK-3$\alpha$ KO fibroblasts versus WT fibroblasts. Differences between groups were determined by unpaired *t* test, and results are expressed as means$\pm$SEM. A probability value of $\leq$0.05 was considered to denote statistical significance. MI indicates myocardial infarction; WT, wild type; KO, GSK-3$\alpha^{(-/-)}$; $\alpha$-SMA, $\alpha$-smooth muscle actin; PCR, polymerase chain reaction.

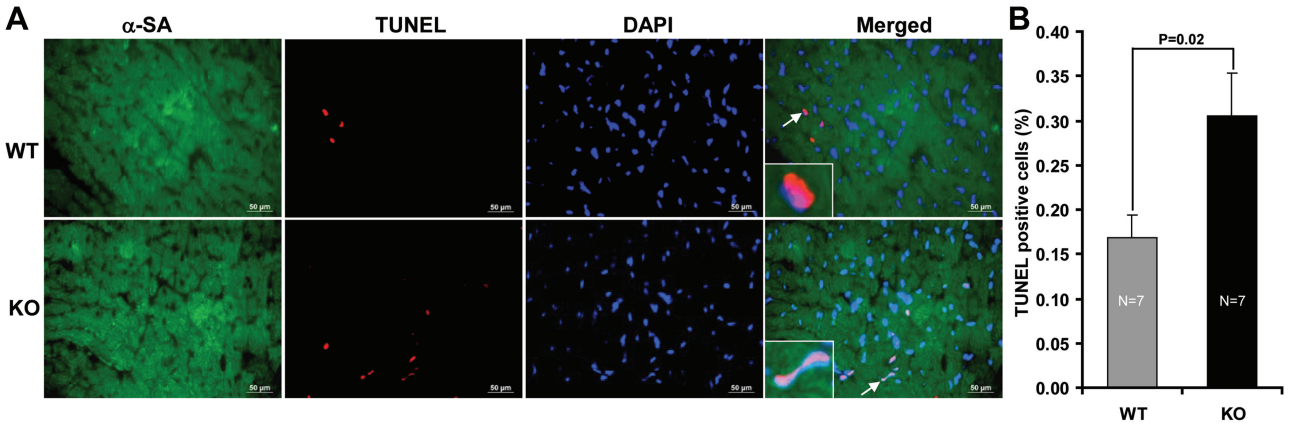


**Figure 6.** GSK-3α deletion leads to increased post-MI apoptosis in the remote myocardium. **A**, Apoptosis in the remote myocardium post-MI. Two-month-old WT and GSK-3α-deficient mice were subjected to MI or sham surgery. At 3 weeks post-MI, apoptotic cells from the remote myocardium were labeled via TUNEL (red). α-SA, a myocyte-specific marker (green), was used to visualize cardiomyocytes and DAPI (blue) was used to label nuclei. Representative images of each marker are shown along with merged image. Arrows highlight a TUNEL-positive nucleus that is within the borders of a α-SA-positive cardiomyocyte. **B**, Quantification of rates of apoptosis is expressed as a percentage of total cells counted. Only TUNEL-positive nuclei colocalized with DAPI and within α-SA-positive cells were counted as apoptotic cardiomyocytes. At least 5000 nuclei in the remote myocardium of each animal were examined. Differences between groups were determined by unpaired *t* test, and results are expressed as means±SEM. A probability value of ≤0.05 was considered to denote statistical significance. TUNEL indicates terminal deoxynucleotidyl-transferase–mediated dUTP nick-end labeling; DAPI, 4,6-diamidino-2-phenylindole; α-SA, α-sarcomeric actin; MI, myocardial infarction; WT, wild type.

fibroblasts (Figure 5D and 5E). Thus, deletion of GSK-3α appears to increase myofibroblast differentiation. As an additional factor that likely promoted the exaggerated fibrosis, we found a significant increase in activation of the profibrotic MAP kinase, p38, in the remote myocardium of the KO (online-only Data Supplement Figure VA and VE).[25,26]

We next asked whether increased cell death in the KO mice could be contributing to the adverse remodeling. To determine the extent of apoptosis, TUNEL-positive nuclei were counted in the noninfarct region. Only cells that were both TUNEL positive and α-sarcomeric actin positive (cardiomyocyte marker), with TUNEL colocalizing with 4,6-diamidino-2-phenylindole, were counted as apoptotic cardiomyocytes. Cardiomyocyte apoptosis was comparable in the WT and KO mice subjected to sham MI surgery (data not shown). However, after MI, the number of TUNEL-positive myocytes was significantly greater in GSK-3α KO mice versus WT mice (Figure 6A and 6B). Thus, GSK-3α deletion significantly increased apoptosis in the remote myocardium of the heart post-MI.

To evaluate this further, we interrogated several signaling pathways implicated in regulating cell death and found significant downregulation of Akt activity in the hearts of KO mice subjected to MI (online-only Data Supplement Figure VA–VC). However, the most striking alterations were in AMPK, with phospho-AMPK being reduced to only 25% of that of the WT level (online-only Data Supplement Figure VA and VD). This would be expected to impair the cardiomyocyte's ability to respond effectively to both ischemic stress and the heart failure environment.

## Deletion of GSK-3α Sensitizes Cardiomyocytes to Ischemia- and Hypoxia-Induced Cell Death

To gain a better understanding of the mechanisms leading to increased ischemic injury in the KO, we also examined apoptosis in the border zone of the infarct at 6 hours post–coronary occlusion. There was a marked increase in apoptosis at this early time point that probably contributed to the increased infarct size in the KO (Figure 7A and 7B). To evaluate this further, we used a hypoxia model in an ex vivo setting. Adult cardiomyocytes from hearts that had not been subjected to MI were isolated from WT and GSK-3α KO mice (8–10 weeks old) as described in Materials and Methods. Cardiomyocytes were exposed to normoxia or hypoxia for 4 hours. Although rates of apoptosis were comparable between WT and GSK-3α KO cardiomyocytes in normoxia, TUNEL-positive nuclei were significantly increased in the KO in response to hypoxia (Figure 7C). This finding was supported by an assay that quantifies cellular release of adenylate kinase, a protein that is only released when cell membrane integrity is compromised (Figure 7D). These data are consistent with a cardiomyocyte autonomous defect that sensitizes GSK-3α KO cardiomyocytes to hypoxic injury.

## Mechanism of Increased Infarct Size in GSK-3α KO Mice

We next examined the possible mechanisms responsible for the increased infarct size and increased sensitivity to hypoxia-induced cardiomyocyte death in the KO mice. There has been an increase in interest in the role of autophagy in the heart's response to ischemic injury. But, despite examining multiple indicators of autophagy (Beclin 1, p62, and the ratio of LC3-II to LC3–1), we found no differences between WT and KO mice subjected to MI (data not shown). However, we found increased association of Bax with the mitochondrial fraction and increased leakage of cytochrome C into the cytosol at 3 weeks post-MI (Figure 8A–8E). Bax and cytochrome C levels were comparable in mitochondrial and cytosolic fraction in WT and KO mice subjected to sham surgery (data not shown). This was not a nonspecific leak, however, because mitochondrial levels of the adenine nucleotide translocase in the KO mice were similar to the WT

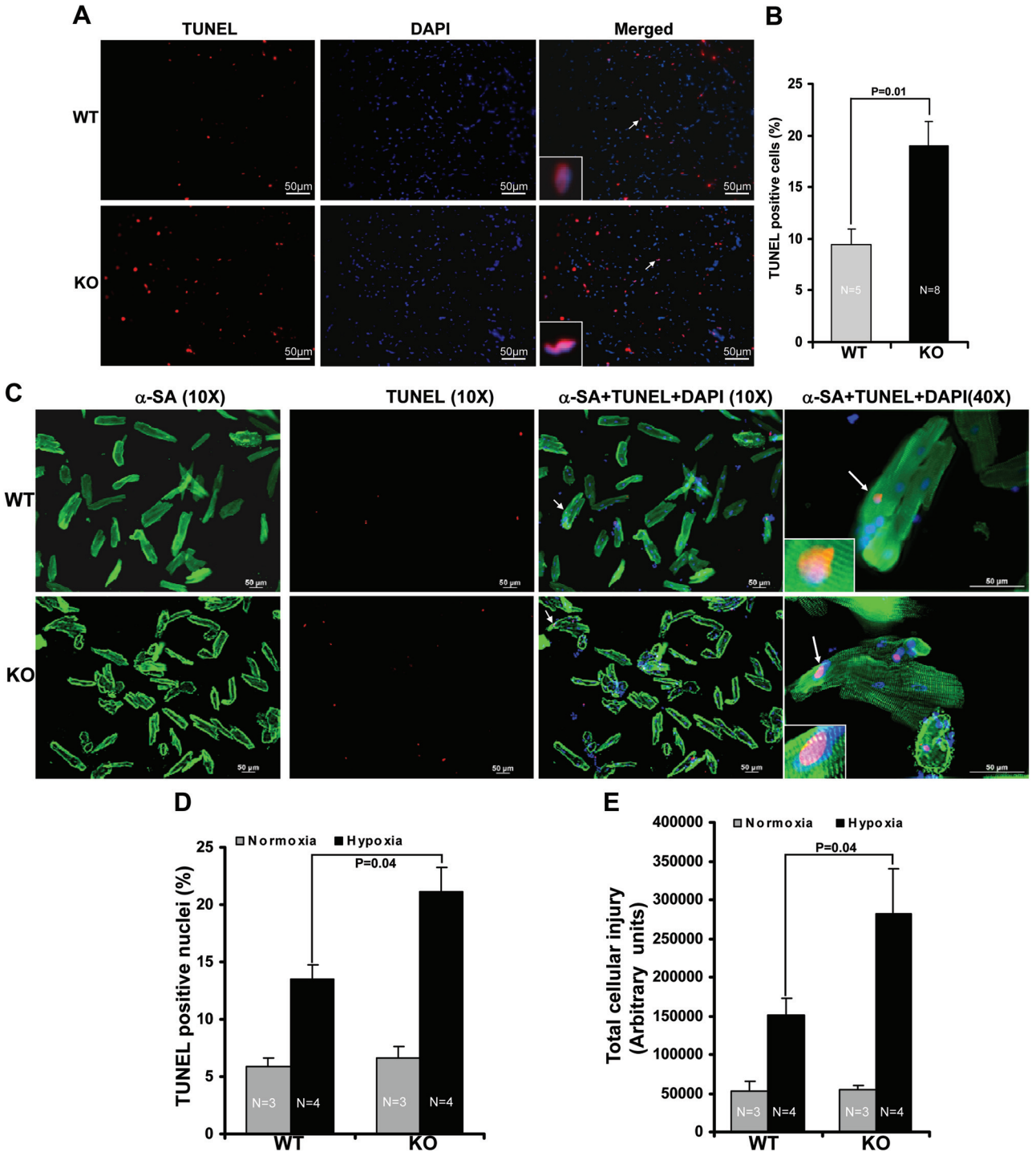


**Figure 7.** Deletion of GSK-3$\alpha$ sensitizes cardiomyocytes to ischemia and hypoxia-induced apoptosis and cellular injury. **A**, Apoptosis in the border zone of the infarct at 6 hours post-MI. Two-month-old WT and GSK-3$\alpha$ KO mice were subjected to MI. At 6 hours post-MI, heart sections were stained via TUNEL (red) and then counterstained with nuclear stain DAPI (blue). Representative images of each marker are shown along with merged image. Arrows highlight a TUNEL-positive nucleus colocalized with DAPI. **B**, Quantification of rates of apoptosis are expressed as a percentage of total cells. TUNEL-positive nuclei were significantly greater in GSK-3$\alpha$ KO mice versus WT mice. **C**, Cardiomyocyte apoptosis after exposure to hypoxia. Adult cardiac myocytes were isolated from 3-month-old WT and GSK-3$\alpha$ KO mice. Cardiomyocytes were exposed to hypoxia for 4 hours, and rates of apoptosis were quantified by TUNEL staining (red). $\alpha$-SA, a myocyte-specific marker (green), was used to visualize cardiomyocytes, and DAPI (blue) was used to label nuclei. Representative images are shown along with merged image. Arrows highlight a TUNEL-positive nucleus that is within the borders of a $\alpha$-SA-positive cardiomyocyte. **D**, Quantification of rates of apoptosis are expressed as a percentage of total cells. The number of TUNEL-positive cells was significantly greater in KO versus WT cardiomyocytes. **E**, As an additional measure of cell death, isolated adult mouse cardiomyocytes were exposed to hypoxia for 4 hours, and cellular toxicity was measured by the release of adenylate kinase (AK) into the cell culture medium as described in Materials and Methods. Differences between groups were determined by unpaired *t* test, and results are expressed as means±SEM. A probability value of ≤0.05 was considered to denote statistical significance. MI indicates myocardial infarction; WT, wild type; KO, GSK-3$\alpha^{(-/-)}$; TUNEL, terminal deoxynucleotidyl-transferase–mediated dUTP nick-end labeling; DAPI, 4,6-diamidino-2-phenylindole; $\alpha$-SA, $\alpha$-sarcomeric actin.

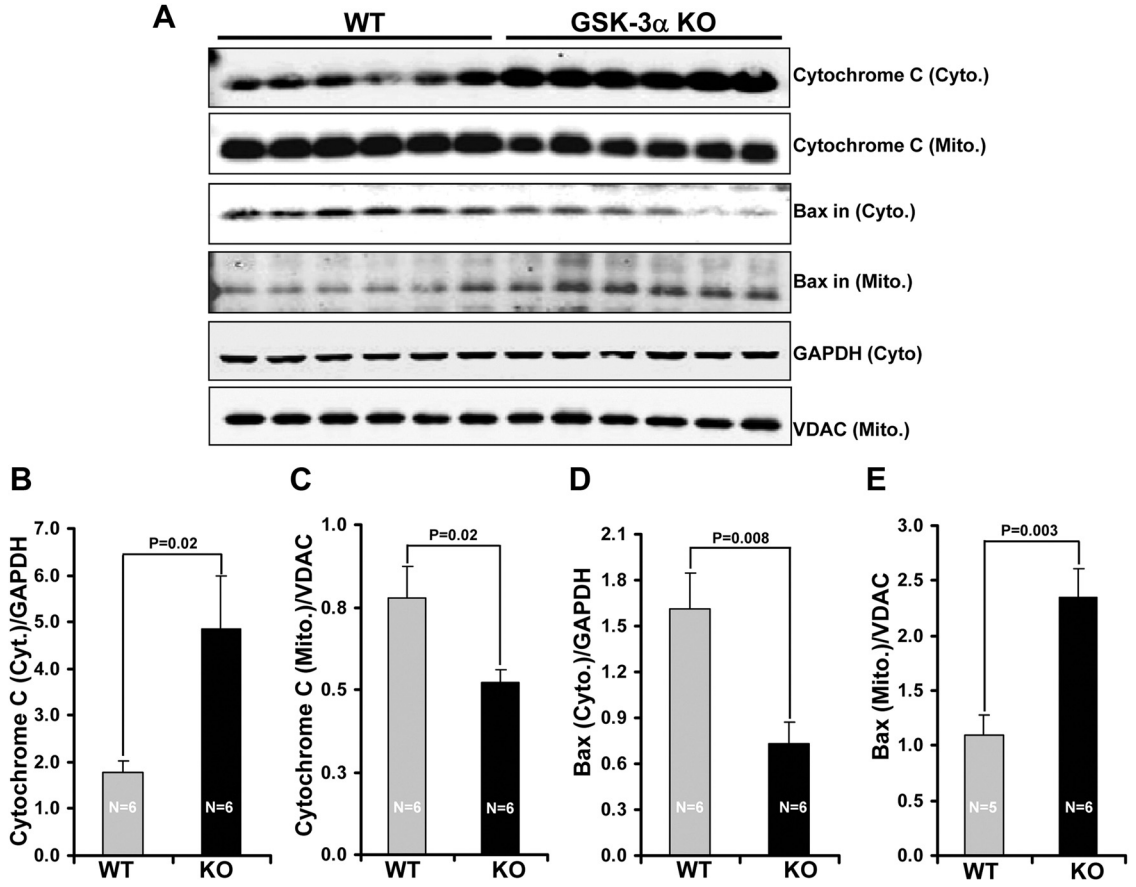


**Figure 8.** Deletion of GSK-3α increased post-MI mitochondrial Bax recruitment and leakage of cytochrome C into the cytosol. **A**, Two-month-old WT and GSK-3α KO mice were subjected to MI or sham surgery for 3 weeks, as described in Materials and Methods. Mitochondrial and cytosolic fraction were analyzed by immunoblotting for mitochondrial Bax recruitment and cytochrome C release into the cytosol, as indicated. **B** through **E**, Bar graphs show normalized fold changes in the leakage of cytochrome C into the cytosol and Bax translocation to the mitochondria. Differences between groups were determined by unpaired *t* test, and results are expressed as means±SEM. A probability value of ≤0.05 was considered to denote statistical significance. MI indicates myocardial infarction; WT, wild type; KO, GSK-3$\alpha^{(-/-)}$; VDAC, voltage-dependent anion channel.

mice. These data suggest that a key mechanism of the protective effects of GSK-3α in reducing ischemic injury is via maintaining the classic proapoptotic factor Bax in an inactive state.

## Discussion

Herein, we have identified a number of novel functions of GSK-3α in the setting of ischemic injury. Most importantly, GSK-3α protects against both ischemic injury and myocardial rupture, the latter being a devastating outcome in patients with MI that is typically fatal. Strikingly, this myocardial protection is seen in a permanent occlusion model of MI, a model in which significant protection is unusual, because very few protective strategies can compensate for total disruption of blood flow to the ischemic region. This finding suggested that GSK-3α might directly modulate cell death. Consistent with that hypothesis, we found a cardiomyocyte-autonomous increase in sensitivity to hypoxic injury in cardiomyocytes isolated from the adult KO. These findings are consistent with our studies in vivo in which there was increased apoptosis in the ischemic border zone in the KO.

Much has been written on the putative role of GSK-3β in promoting ischemic injury,[27–31] but, to our knowledge, only one report has addressed the role of GSK-3α.[32] The authors of that study used RNA interference in neonatal rat cardiomyocytes and concluded that the knockdown of GSK-3β was protective against ischemic injury, but that the knockdown of GSK-3α was not. However, the experiments were structured to determine whether the knockdown of GSK-3α was protective and not whether knockdown was detrimental. We believe that our data demonstrate definitively that the α-isoform acts to limit ischemic injury. It is noteworthy that, although infarct size was significantly increased in the GSK-3α KO mice, the magnitude of the difference in MI size between WT and KO mice probably underestimates the true difference because of the excess early deaths due to rupture in the KO mice. In all likelihood, the mice that died of rupture had larger infarcts, but, in most cases, the tissue was not able to be processed for MI size determination because of the relatively long lag times between death and our discovering that the animals had died.

The GSK-3α KO mice had significantly more remodeling post-MI than the WT mice. Although it is possible that this is solely due to the larger infarct size in the KO mice, the data suggest that other processes play a role in driving remodeling. For example, the ongoing cell loss due to apoptosis in vivo in

the remote myocardium and the border zone of the KO mice was significantly greater than in the WT mice. This, combined with the increased hypoxia-induced cell death in cardiomyocytes isolated from the KO mice, suggest that the KO cardiomyocytes are inherently less able to adapt to ischemic stress. Thus, we believe that the ongoing remodeling is not simply due to the initial insult, but is also driven by continued cell loss.

What was also very notable about the KOs was the marked increase in fibrosis in the remote myocardium following MI. Indeed, on average, fully 15% of the remote myocardium in the KO mice was replaced by fibrosis in comparison with only 4% in the WT. Consistent with this, $\alpha$-SMA expression, which is a marker of the transition of the fibroblast to the more profibrotic myofibroblast, was increased. Again, we believe that this exaggerated fibrosis is not simply due to the larger infarcts in the KO, because fibroblasts isolated from KO hearts that had not been exposed to stress more readily differentiated into myofibroblasts than did WT fibroblasts. These data suggest that a fibroblast autonomous effect of the deletion of GSK-3$\alpha$ drives myofibroblast transformation and fibrosis.

In summary, we have identified GSK-3$\alpha$ as a key signaling factor in the response to ischemia. In the absence of GSK-3$\alpha$, infarct size is increased, as is cardiac rupture and death. Post-MI remodeling is profound, leading to LV dilatation, dysfunction, and striking fibrotic remodeling. It remains unclear as to the proximate mechanisms by which deletion of GSK-3$\alpha$ drives Bax translocation to mitochondria and the constitutive release of cytochrome C. The mechanism could be either direct (eg, via phosphorylation) or indirect (eg, due to the marked dysregulation of Akt and AMPK seen in the KO mice). Unbiased proteomic studies will probably be required to address this complex issue.

From a clinical perspective, the GSK-3 family of kinases has been implicated in a host of disease states, and, as noted, therapeutics targeting the family are in development. Given the fact that, at least at present, isoform-specific inhibitors of GSK-3$\beta$ have not been developed, we suggest caution in going forward with drug development targeting this family of kinases.



## Acknowledgments

We thank Shi Pan and Shey-Shing Sheu for professional advice and Renata Skubutyte and Makarand V. Risbud for help with the hypoxia experiment and hypoxia chamber. We also thank Jianliang Song and Joseph Y Cheung for help with adult cardiomyocyte isolation.

## Sources of Funding

This work was supported by grants HL061688 and HL091799 from the U.S. National Heart Lung and Blood Institute and by donations from The Kahn Foundation and the Scarperi family (to T.F.), the Canadian Institutes of Health Research Grants MOP12858 and 74711 (to J.R.W.).

## Disclosures

None

## References

1. Velagaleti RS, Pencina MJ, Murabito JM, Wang TJ, Parikh NI, D'Agostino RB, Levy D, Kannel WB, Vasan RS. Long-term trends in the incidence of heart failure after myocardial infarction. *Circulation*. 2008; 118:2057–2062.
2. Sutton MG, Sharpe N. Left ventricular remodeling after myocardial infarction: pathophysiology and therapy. *Circulation*. 2000;101: 2981–2988.
3. Gajarsa JJ, Kloner RA. Left ventricular remodeling in the post-infarction heart: a review of cellular, molecular mechanisms, and therapeutic modalities. *Heart Fail Rev*. 2011;16:13–21.
4. Woulfe KC, Gao E, Lal H, Harris D, Fan Q, Vagnozzi R, DeCaul M, Shang X, Patel S, Woodgett JR, Force T, Zhou J. Glycogen synthase kinase-3$\beta$ regulates post–myocardial infarction remodeling and stress-induced cardiomyocyte proliferation in vivo. *Circ Res*. 2010;106: 1635–1645.
5. Vigneron F, Dos Santos P, Lemoine S, Bonnet M, Tariosse L, Couffinhal T, Duplaa C, Jaspard-Vinassa B. GSK-3$\beta$ at the crossroads in the signalling of heart preconditioning: implication of mTOR and Wnt pathways. *Cardiovasc Res*. 2011;90:49–56.
6. Forster K, Richter H, Alexeyev MF, Rosskopf D, Felix SB, Krieg T. Inhibition of glycogen synthase kinase 3beta prevents peroxide-induced collapse of mitochondrial membrane potential in rat ventricular myocytes. *Clin Exp Pharmacol Physiol*. 2010;37:684–688.
7. Webb IG, Sicard P, Clark JE, Redwood S, Marber MS. Myocardial stress remodelling after regional infarction is independent of glycogen synthase kinase-3 inactivation. *J Mol Cell Cardiol*. 2010;49:897–900.
8. Zhou J, Lal H, Chen X, Shang X, Song J, Li Y, Kerkela R, Doble BW, MacAulay K, DeCaul M, Koch WJ, Farber J, Woodgett J, Gao E, Force T. GSK-3alpha directly regulates beta-adrenergic signaling and the response of the heart to hemodynamic stress in mice. *J Clin Invest*. 2010;120:2280–2291.
9. Ko R, Jang HD, Lee SY. GSK3beta inhibitor peptide protects mice from LPS-induced endotoxin shock. *Immune Netw*. 2010;10:99–103.
10. Hu S, Begum AN, Jones MR, Oh MS, Beech WK, Beech BH, Yang F, Chen P, Ubeda OJ, Kim PC, Davies P, Ma Q, Cole GM, Frautschy SA. GSK3 inhibitors show benefits in an Alzheimer's disease (AD) model of neurodegeneration but adverse effects in control animals. *Neurobiol Dis*. 2009;33:193–206.
11. Dokken BB, Sloniger JA, Henriksen EJ. Acute selective glycogen synthase kinase-3 inhibition enhances insulin signaling in prediabetic insulin-resistant rat skeletal muscle. *Am J Physiol Endocrinol Metab*. 2005;288:E1188–E1194.
12. Bhat RV, Budd Haeberlein SL, Avila J. Glycogen synthase kinase 3: a drug target for CNS therapies. *J Neurochem*. 2004;89:1313–1317.
13. Gao E, Lei YH, Shang X, Huang ZM, Zuo L, Boucher M, Fan Q, Chuprun JK, Ma XL, Koch WJ. A novel and efficient model of coronary artery ligation and myocardial infarction in the mouse. *Circ Res*. 2010; 107:1445–1453.
14. Chen X, Shevtsov S, Hsich E, Cui L, Haq S, Aronovitz MJ, Kerkela R, Molkentin JD, Liao R, Salomon R, Patten RD, Force T. The $\beta$-catenin/T-cell factor/lymphocyte enhancer factor signaling pathway is required for normal and stress-induced cardiac hypertrophy. *Mol Cell Biol*. 2006; 26:4462–4473.
15. Jenkins C, Moir S, Chan J, Rakhit D, Haluska B, Marwick TH. Left ventricular volume measurement with echocardiography: a comparison of left ventricular opacification, three-dimensional echocardiography, or both with magnetic resonance imaging. *Eur Heart J*. 2009;30:98–106.
16. Qin JX, Shiota T, Thomas JD. Determination of left ventricular volume, ejection fraction, and myocardial mass by real-time three-dimensional echocardiography. *Echocardiography*. 2000;17:781–786.
17. Most P, Seifert H, Gao E, Funakoshi H, Volkers M, Heierhorst J, Remppis A, Pleger ST, DeGeorge BR Jr, Eckhart AD, Feldman AM, Koch WJ. Cardiac S100A1 protein levels determine contractile performance and propensity toward heart failure after myocardial infarction. *Circulation*. 2006;114:1258–1268.
18. Kerkela R, Kockeritz L, Macaulay K, Zhou J, Doble BW, Beahm C, Greytak S, Woulfe K, Trivedi CM, Woodgett JR, Epstein JA, Force T, Huggins GS. Deletion of GSK-3beta in mice leads to hypertrophic cardiomyopathy secondary to cardiomyoblast hyperproliferation. *J Clin Invest*. 2008;118:3609–3618.
19. Zhou YY, Wang SQ, Zhu WZ, Chruscinski A, Kobilka BK, Ziman B, Wang S, Lakatta EG, Cheng H, Xiao RP. Culture and adenoviral infection of adult mouse cardiac myocytes: methods for cellular genetic physiology. *Am J Physiol Heart Circ Physiol*. 2000;279:H429–H436.
20. Kerkela R, Grazette L, Yacobi R, Iliescu C, Patten R, Beahm C, Walters B, Shevtsov S, Pesant S, Clubb FJ, Rosenzweig A, Salomon RN, Van

Etten RA, Alroy J, Durand JB, Force T. Cardiotoxicity of the cancer therapeutic agent imatinib mesylate. *Nat Med*. 2006;12:908–916.
21. Elrod JW, Wong R, Mishra S, Vagnozzi RJ, Sakthievel B, Goonasekera SA, Karch J, Gabel S, Farber J, Force T, Brown JH, Murphy E, Molkentin JD. Cyclophilin D controls mitochondrial pore-dependent Ca(2+) exchange, metabolic flexibility, and propensity for heart failure in mice. *J Clin Invest*. 2010;120:3680–3687.
22. Agocha AE, Eghbali-Webb M. A simple method for preparation of cultured cardiac fibroblasts from adult human ventricular tissue. *Mol Cell Biochem*. 1997;172:195–198.
23. Doble BW, Patel S, Wood GA, Kockeritz LK, Woodgett JR. Functional redundancy of GSK-3alpha and GSK-3beta in Wnt/beta-catenin signaling shown by using an allelic series of embryonic stem cell lines. *Dev Cell*. 2007;12:957–971.
24. Swaney JS, Roth DM, Olson ER, Naugle JE, Meszaros JG, Insel PA. Inhibition of cardiac myofibroblast formation and collagen synthesis by activation and overexpression of adenylyl cyclase. *Proc Natl Acad Sci U S A*. 2005;102:437–442.
25. Rose BA, Force T, Wang Y. Mitogen-activated protein kinase signaling in the heart: angels versus demons in a heart-breaking tale. *Physiol Rev*. 2010;90:1507–1546.
26. Zhang S, Weinheimer C, Courtois M, Kovacs A, Zhang CE, Cheng AM, Wang Y, Muslin AJ. The role of the Grb2–p38 MAPK signaling pathway in cardiac hypertrophy and fibrosis. *J Clin Invest*. 2003;111:833–841.
27. Nishihara M, Miura T, Miki T, Tanno M, Yano T, Naitoh K, Ohori K, Hotta H, Terashima Y, Shimamoto K. Modulation of the mitochondrial permeability transition pore complex in GSK-3beta-mediated myocardial protection. *J Mol Cell Cardiol*. 2007;43:564–570.
28. Zhu J, Rebecchi MJ, Glass PS, Brink PR, Liu L. Cardioprotection of the aged rat heart by GSK-3beta inhibitor is attenuated: age-related changes in mitochondrial permeability transition pore modulation. *Am J Physiol Heart Circ Physiol*. 2011;300:H922–H930.
29. Xi J, Tian W, Zhang L, Jin Y, Xu Z. Morphine prevents the mitochondrial permeability transition pore opening through NO/cGMP/PKG/Zn2+/GSK-3beta signal pathway in cardiomyocytes. *Am J Physiol Heart Circ Physiol*. 2010;298:H601–H607.
30. Miura T, Tanno M. Mitochondria and GSK-3beta in cardioprotection against ischemia/reperfusion injury. *Cardiovasc Drugs Ther*. 2010;24:255–263.
31. Wong R, Aponte AM, Steenbergen C, Murphy E. Cardioprotection leads to novel changes in the mitochondrial proteome. *Am J Physiol Heart Circ Physiol*. 2010;298:H75–H91.
32. Juhaszova M, Zorov DB, Kim SH, Pepe S, Fu Q, Fishbein KW, Ziman B, Wang S, Ytrehus K, Antos CL, Olson EN, Sollott SJ. Glycogen synthase kinase-3beta mediates convergence of protection signaling to inhibit the mitochondrial permeability transition pore. *J Clin Invest*. 2004;113:1535–1549.

## CLINICAL PERSPECTIVE

Occlusion of a coronary artery typically leads to ST-segment elevation myocardial infarction, for which percutaneous coronary intervention (PCI) or, if PCI is not available, thrombolytics, are the standard of care. The pathways that determine the amount of injury following occlusion of a coronary artery are not clear. If the components of those pathways could be identified, novel therapeutics targeting them could be created. This might be of particular importance when PCI is not readily available or when there will be delays in accessing a catheterization laboratory. Herein, we identify a single factor, a protein kinase known as glycogen synthase kinase-3α (GSK-3α), that modulates injury post–coronary occlusion. In the absence of GSK-3α, infarct size is larger, and mortality, primarily because of cardiac rupture, is increased. Long-term, adverse remodeling including profound fibrosis, and contractile dysfunction leading to heart failure, are more pronounced. It is uncommon to see significant cardioprotection in the setting of a permanent coronary artery occlusion because of the complete absence of flow, but our studies suggest that strategies promoting activation of GSK-3α might prove beneficial, even in the setting of an occluded vessel.